Size-Dependent Photoluminescence Efficiency of Silicon Nanocrystal Quantum Dots

Size-Dependent Photoluminescence Efficiency of Silicon Nanocrystal Quantum Dots

Yixuan Yu,[†] Gang Fan,[†] Andrea Fermi,[‡] Raffaello Mazzaro,[ǂ] Vittorio Morandi,[ǂ] Paola Ceroni,[‡] Detlef-M. Smilgies,[‖] Brian A. Korgel[†*]

[†] McKetta Department of Chemical Engineering and Texas Materials Institute, The University of Texas at Austin, Austin, TX, 78712-1062, USA.

[‡] Department of Chemistry "G. Ciamician", University of Bologna, Via Selmi 2, 40126 Bologna, Italy.

[ǂ] Institute for Microelectronics and Microsystems (IMM) Section of Bologna, National Research Council (CNR), Via Gobetti 101, 40129 Bologna, Italy.

[‖] Cornell High Energy Synchrotron Source (CHESS), Cornell University, Ithaca, NY 14853, USA.

*Corresponding author: korgel@che.utexas.edu

ABSTRACT

Photoluminescence (PL) spectra were measured for dodecene-capped Si nanocrystals with a wide range of average diameter, from 1.8 nm to 9.1 nm. Nanocrystals larger than 3 nm exhibited relatively high PL quantum yields of 30% to 45%. Smaller nanocrystals exhibited lower quantum yields that decreased significantly with reduced size. Because smaller nanocrystals also have lower optical absorption there is a significant biasing of the PL spectra by the larger nanocrystals. We show that with proper accounting of polydispersity and size-dependent quantum yields and optical absorption, the effective mass approximation (EMA) accurately estimates the average diameter of silicon (Si) nanocrystals from experimentally-determined PL

emission peak energies. A finite confinement model is presented that explains the decreased PL quantum yields of the smaller diameter nanocrystals.

INTRODUCTION

The synthesis of silicon (Si) nanocrystals has advanced significantly in the past few years.[1-14] Now it is possible to obtain significant quantities of crystalline Si nanocrystals with a wide range of sizes, sufficient uniformity to form superlattices, and well-characterized surface ligand passivation that largely prevents oxidation.[15-17] Si nanocrystals have been shown to be efficient light-emitters with photoluminescence (PL) quantum yields as high as 60%,[10,18] and color that can be widely turned from the near infrared towards the blue end of the spectrum.[9,19-21] Si nanocrystals have been explored in a variety of light-emitting applications, such as fluorescence bioimaging contrast agents[2,22,23] light-emitting diodes (LED),[24-26] and luminescent solar concentrators.[27] Nonetheless, there still remains uncertainty about how the emission wavelength correlates with Si nanocrystal size.[4,28,29] This is due to differences in surface passivation and uncertainty in sizing of the nanocrystals in various studies. Here, we examine nanocrystals with a wide range of sizes prepared using the same synthetic and passivation approach and accurately measure the size of the nanocrystals using both transmission electron microscopy (TEM) and small angle X-ray scattering (SAXS), which is especially important for the nanocrystals smaller than ~3 nm in diameter.

The effective mass approximation (EMA) has been used often as a convenient method to estimate the size of semiconductor nanocrystal quantum dots from optical spectra.[30,31] The EMA has been reported to overestimate the optical gap for nanocrystals in the smaller size range (< 3 nm).[32-37] Alternative approaches to calculating the size-dependent optical gap of Si nanocrystals have included modified versions of the EMA[34] and quantum mechanical models that introduce

oxygen-related surface states.[36] However, without accurate sizing of the nanocrystals, the accuracy of these models for predicting the size dependence of the PL peak energy cannot be assessed. Here, we measure the average diameter and the size distribution of dodecene-capped Si nanocrystals ranging in diameter from 1.8 nm to 9.1 nm using TEM and small angle X-ray scattering (SAXS) and find good agreement between the size-dependent optical gap calculated using the EMA and the experimentally measured peak PL energies, *provided that the size-dependent optical absorption and PL quantum yields are properly accounted for*. For the small nanocrystal size range, SAXS is a more accurate method of measuring the average size and size distribution of the nanocrystals than TEM. Although very high resolution TEM images of Si nanocrystals have been obtained in a couple of instances,[20,37] it is experimentally difficult to measure accurately the diameter of Si nanocrystals using TEM because of the quality of the samples and the low imaging contrast of Si, especially when the size of the nanocrystals is small. The Si nanocrystals studied here exhibit bright light emission and have sufficient size uniformity to use SAXS to measure the size and size distribution of the samples, including the nanocrystals of the smallest diameter.

EXPRIMENTAL DETAILS

Materials FOx-16 was purchased from Dow Corning. 1-dodecene (98%) was purchased from Sigma-Aldrich. Ethanol, toluene, chloroform, and hydrochloric acid (HCl, 37.5%) were from Fisher Scientific. Hydrofluoric acid (HF, 48%) was obtained from EMD chemicals. Deionized (DI) water was obtained using a Barnstead Nanopure Filtration System (17 MΩ resistance).

Synthesis of Si nanocrystals Si nanocrystals were obtained via thermal decomposition of HSQ, followed with etching and hydrosilylation.[7,15,20] In a typical synthesis, FOX-16 is loaded into a round bottle flask and the solvent is evaporated on a Schlenk line for 4 hr to generate glassy hydrogen silsesquioxane (HSQ), which was subsequently heated to 1100-1400ºC for 1 hr under hydrogen/nitrogen (7%/93%) forming gas flow. Higher temperature produces larger nanocrystals. The product, containing Si nanocrystals (10% in weight) embedded in SiO_2 matrix (90% in weight), was ground with agate mortar and pestle for 10 min and shaken in a wrist-action shaker for 9 hr with 3 mm borosilicate glass beads. 1 gram of the ground powder were etched in 3 ml 37.5% HCl and 30 ml 48% HF in dark for 4-6 hours to yield hydride-terminated Si nanocrystal. These nanocrystals were isolated by centrifugation at 8000 rpm for 5 min and rinsed once with DI water, twice with ethanol, and once with chloroform, and finally dispersed in 1-dodecene and heated at 190ºC for 12 hr after 3 freeze-pump-thaw cycles to complete surface passivation.

Si nanocrystals were cleaned by centrifugation at 8000 rpm for 5 min to precipitate poorly capped nanocrystals. The supernatant was mixed with ethanol and centrifuged at 8000 rpm for 5 min to precipitate nanocrystals that were redispersed in toluene. The size distributions of nanocrystals were narrowed with multistep size-selective precipitation. After size-selection, each nanocrystals sample contains 10-50 mg of material. The nanocrystals were rinsed four times by using toluene/ethanol solvent combination, and finally dispersed in toluene at a concentration of 5 mg/mL until further use.

Materials characterization Solution Small Angle X-ray scattering (SAXS) was performed on D1 beam line of the Cornell High Energy Synchrotron Source (CHESS) using monochromatic X-ray radiation with a wavelength of 1.154 Å. A fiber-coupled CCD camera

(MedOptics) of 1024 × 1024 pixels with pixel size of 46.9 μm × 46.9 μm and 14-bit dynamic range per pixel was used to acquire the SAXS pattern images. The typical sample-to-detector distance was 500-700 mm, determined by using silver behenate powder as a calibration standard. In a typical measurement, toluene dispersion of nanocrystals at a concentration of 5 mg/mL is loaded into a capillary tube, which is aligned perpendicular to the X-ray beam. The typical exposure time for solution SAXS is 600 sec. The data are fit to the calculated scattering intensity expected for a collection of non-interacting solid spheres:[38]

$$I(q) \propto \int_0^\infty N(R)P(qR)R^6 dR \quad (1)$$

where $N(R)$ is the nanocrystal size distribution, which is taken to be Gaussian with average radius $\bar{R}$ and standard deviation σ,

$$N(R) = \frac{1}{\sigma 2\pi} \exp\left[\frac{-(R-\bar{R})^2}{2\sigma^2}\right] \quad (2)$$

and the form factor $P(qR)$, is for homogenous spheres,

$$P(qR) = \left[3\frac{\sin(qR) - qR\cos(qR)}{(qR)^3}\right]^2 \quad (3)$$

Transmission electron microscopy (TEM) images were acquired using a FEI Tecnai Biotwin TEM operated at 80 kV accelerating voltage. Nanocrystals were drop cast onto 200 mesh carbon-coated copper grids for imaging (Electron Microsopy Science). X-ray diffraction (XRD) was performed using a Rigaku R-Axis Spider Diffractometer using Cu Kα radiation (λ=0.15418 nm). Nanocrystals were dried on a glass slide and placed onto a nylon loop. Two-dimensional diffraction data were collected for 60 min while rotating the sample stage at 10° per minute. 2D diffraction data were radially integrated with 2DP Spider software (version 1.0, Rigaku Americas Corp.)

Photoluminescence (PL) spectra in the UV-visible wavelength range were acquired on a Varian Cary Eclipse fluorescence spectrophotometer and in the UV-visible-NIR wavelength range on a Fluorolog-3 spectrophotometer (Horiba Jobin Yvon) with InGaAs photomultiplier tube, using 350 nm as the excitation wavelength for visible PL and 400 nm for NIR emission. A Hamamatsu H10330-45 detector was used during the time correlated single photon counting (TCSPC) measurement for PL decay, using 371 nm NanoLED laser as the excitation source. The PL quantum yield is the ratio of the number of emitted photons to the number of absorbed photons and can be estimated by comparing the sample PL intensity and the absorbance at excitation wavelength to those of a standard dye with known PL quantum yield. PL quantum yields for nanocrystals smaller than 3 nm were estimated relative to Rhodamine 101 in anhydrous ethanol (Φ=1). Edinburgh FLS920 spectrofluorometer equipped with a Ge-detector is used to measure the NIR quantum yield. NIR emission dyes HITCI (1,1',3,3,3',3'-hexamethylindotricarbocyanine iodide) in EtOH, Φ=0.30 and $[Ru(bpy)_3]Cl_2$ Φ=0.040 in air-equilibrated aqueous solution are used as the standards. Emission spectra were corrected for detector sensitivity in the 550-1200 nm region by using a calibrated lamp. NIR quantum yields were verified with the absolute method developed by de Mello *et al.*[39] using an integrating sphere to determine the relative numbers of emitted and absorbed photons. Emission lifetimes in NIR range were recorded using a Varian phosphorimeter with excitation at 350 nm, λem =850 nm or emission peak wavelength.

X-ray photoelectron spectroscopy (XPS) was measured with a Kratos Axis Ultra XPS, utilizing monochromatic Al K_α X-rays ($h\nu$ = 1486.5 eV) at 150 W (10 mA and 15 kV). The instrument work function is calibrated to show a binding energy (BE) of 368.3 eV for the Ag $3d_{5/2}$ line for metallic silver. Spectra were charge-corrected to the main line of the carbon 1s

spectrum (284.5 eV). High resolution XPS spectra were collected with a pass energy of 20 eV, at a 0.1 eV step. Casa XPS analysis software (Version 2.3.16 PR 1.6) was used for peak deconvolution.

RESULTS AND DISCUSSION

Si nanocrystals. Figure 1 shows TEM images of dodecene-capped Si nanocrystals used in the study. The average diameter of the nanocrystals ranged from as small as 1.8 nm up to 9.1 nm and all of the nanocrystals were crystalline with diamond cubic crystal structure, as the XRD data in Figure 3 show. The diffraction peaks are broader for the smaller nanocrystals as expected. TEM can be used to accurately determine the size of the larger nanocrystals but not for the smaller nanocrystals (less than ~3 nm) because the image contrast is too low. The TEM images show that the smaller nanocrystals are relatively uniform in size though, making it possible to use SAXS to determine their size. Figure 2 shows Porod plots[40] of the SAXS data of Si nanocrystals dispersed in toluene. By fitting Eqns (1)-(3) to these data, the average diameter of and standard deviation of the nanocrystal size distribution were determined. TEM was used to determine more precisely the size and size distribution of the larger nanocrystals, *e.g.* 9.1 nm, because their significant faceting makes the assumption of a spherical particle shape inaccurate.

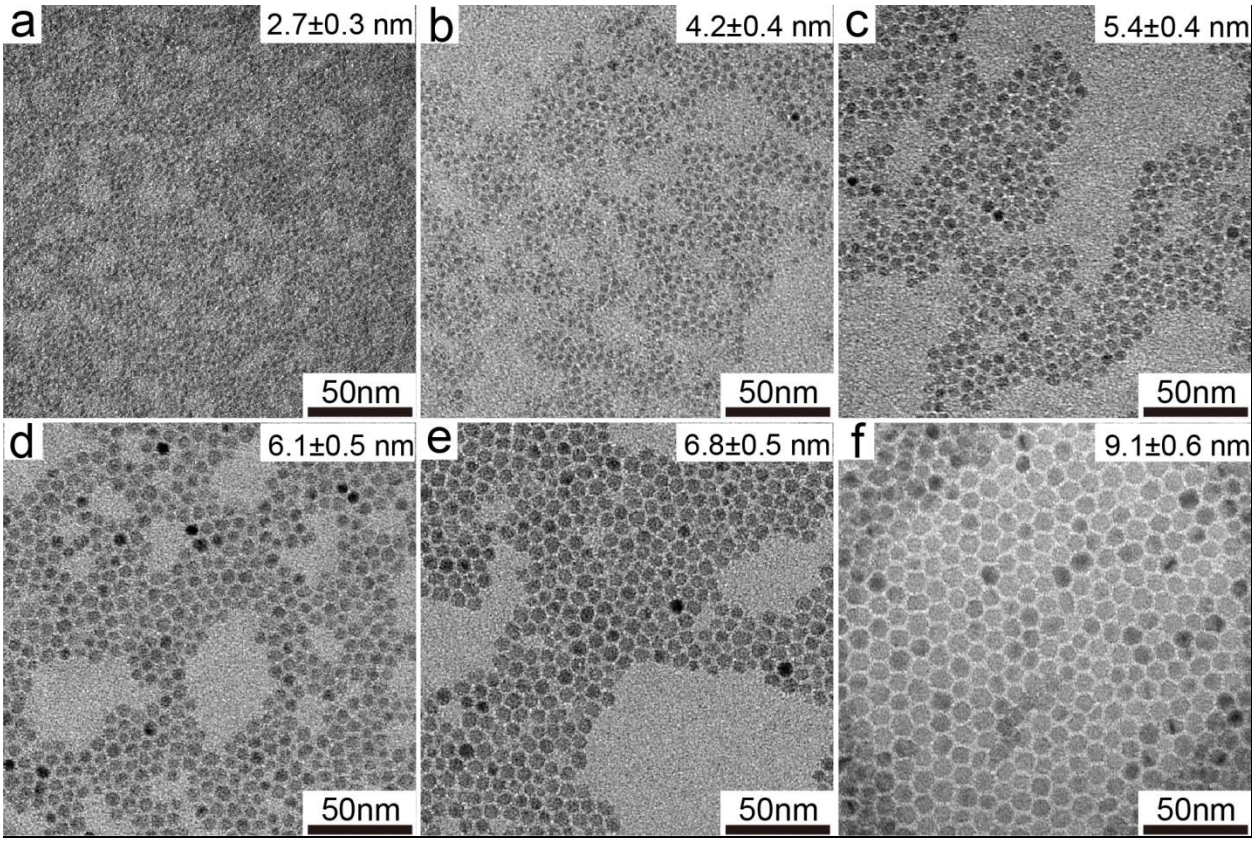

Figure 1. TEM images of dodecene-passivated Si nanocrystals used in the study with average diameter and standard deviation noted in the insets.

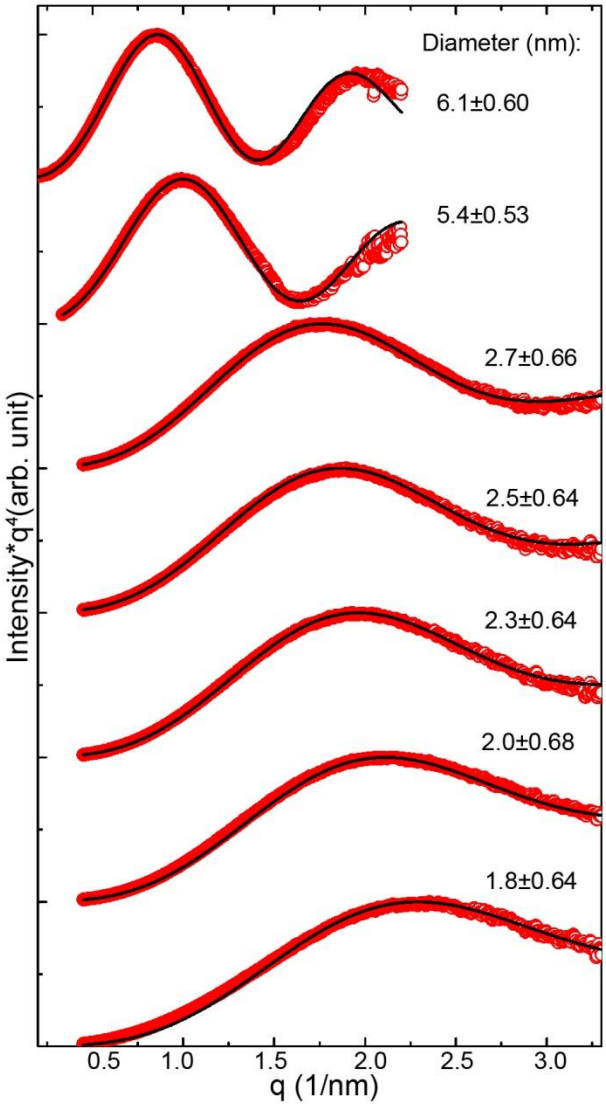

Figure 2. Porod plots of SAXS data for the dodecene-capped Si nanocrystals used in the study dispersed in toluene (red circles). The black curves are the best fits of Eqns (1)-(3) to the data (red circles) to obtain the average diameter and standard deviation values shown for each data set.

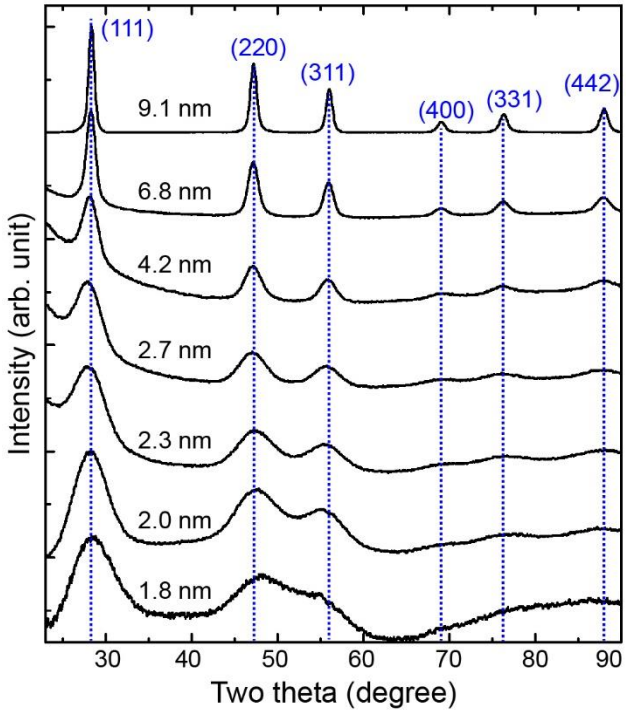

Figure 3. XRD of Si nanocrystals with the indicated average diameter. The diffraction peaks are indexed to diamond cubic Si with blue labels (PDF#027–1402, a=b=c=5.43088 Å). The X-ray wavelength was $\lambda = 0.15418$ nm for Cu K_α radiation

The PL emission spectra of the dodecene-capped Si nanocrystals are shown in Figure 4a. The nanocrystals span a wide range of size and the color the samples extends from visible to near infrared (NIR) wavelengths. For Si nanocrystals, the PL peak energy provides a convenient measure of the optical gap. Because Si has an indirect bandgap, there are no exciton peaks in the absorbance spectra (Figure S5) and it is difficult to determine precisely the absorption edge because the low density of states make the optical absorption near the absorption edge extremely weak.[20,41] The EMA for the energy of the optical gap E(d), of nanocrystals with diameter *d*, is:[33]

$$\mathrm{E(d)} = E_g + \frac{h^2\pi^2}{2d^2}\left(\frac{1}{m_e^*} + \frac{1}{m_h^*}\right) - \frac{1.786e^2}{\varepsilon d} \qquad (4)$$

E_g is the bulk band gap of Si. Figure 4b shows a plot of E(d) calculated using the EMA assuming that the nanocrystals are perfectly uniform without any polydispersity compared with the experimentally measured PL peak energies for the nanocrystals. For nanocrystals with diameters larger than ~3 nm, there is good agreement between the EMA values and the experimental values. But when the nanocrystals were small—less than ~3 nm in diameter—the EMA significantly overestimates the optical gap. As shown below, this is due to the effect of the polydispersity in the sample, which must be taken in to account. It is also worth noting that our PL data are consistent with the results of Wolkin et al. (green triangles in Figure 4b), which have been attributed to the generation of Si=O related radiative recombination centers.[36] In this work, we do not try to rule out that possibility of Si=O related radiative recombination centers playing a role, but rather provide an alternative explanation that is also consistent with the data.

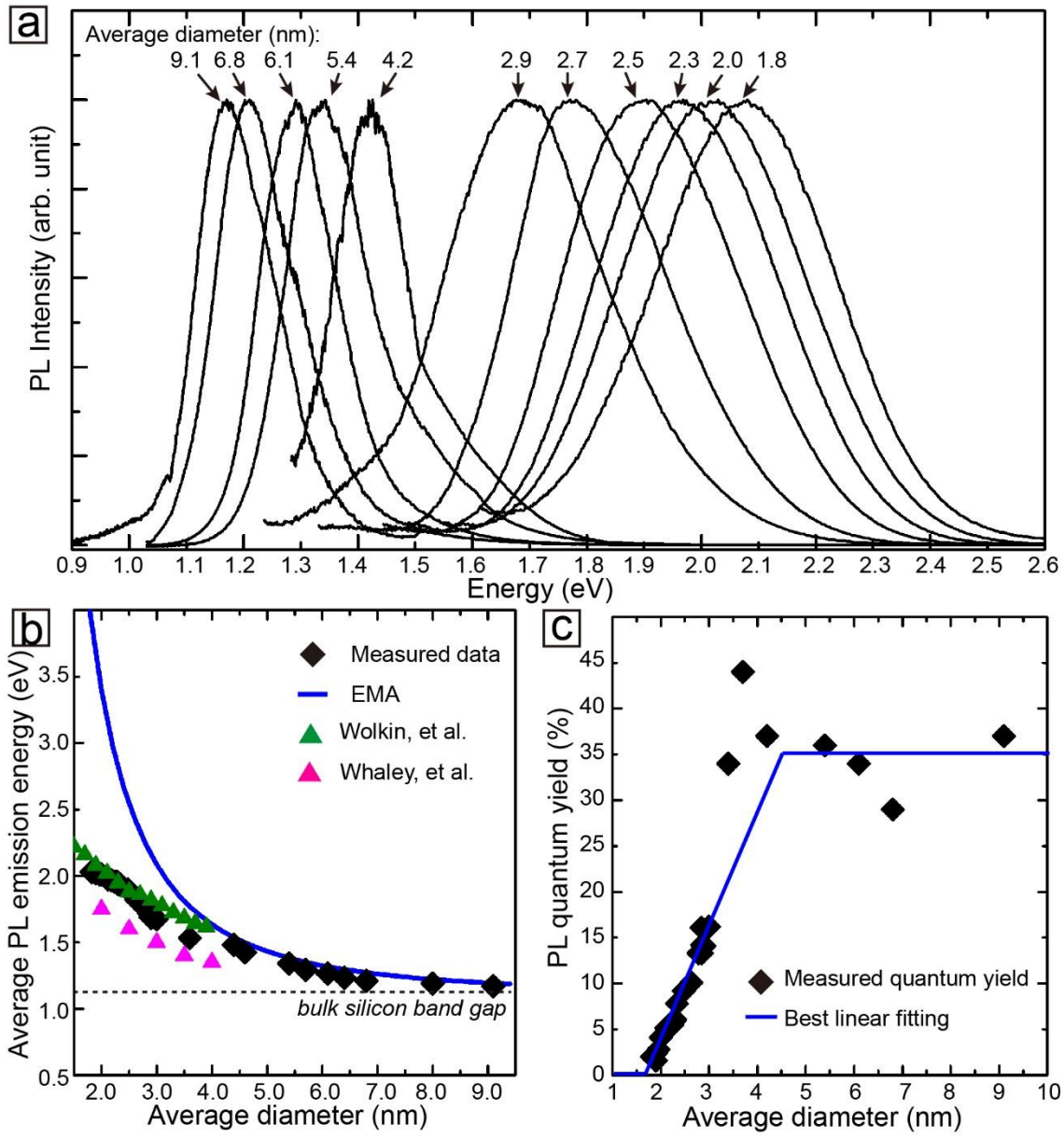

Figure 4. (a) PL spectra of Si nanocrystals with various average diameters and maximum intensity normalized to a constant. The excitation wavelength for nanocrystals smaller than 3 nm is 350 nm, while larger Si nanocrystals are excited at 400 nm (b) Peak PL emission energy plotted versus the average nanocrystal diameter, in which the blue curve shows the optical gap calculated using the EMA assuming no distribution in nanocrystal size (Eqn. 4). The dotted line provides a reference for the bulk band gap of Si (1.12 eV). The average diameters of nanocrystals larger than 6 nm were determined from TEM images, while the others are

determined by fitting solution SAXS data. (c) PL quantum yields of Si nanocrystals with various diameters.. The blue line is a linear fit of the data.

Both the optical absorption and the PL quantum yield are size dependent.[11,20,28] The measured size dependence of the PL quantum yield is shown in Figure 4c. The PL quantum yield $QY(d)$, of the larger nanocrystals is roughly independent of size, but decreases when the diameter is smaller than about 4.5 nm:

$$QY(d) = \begin{cases} 0, & d < 1.73\ nm \\ 0.125d - 0.216, & 1.73 \le d \le 4.5 \\ 0.35, & d > 4.5 \end{cases} \quad (5)$$

The extinction coefficient $\varepsilon(d)$ is also size-dependent. Various semiconductor nanocrystals have been shown to have a similar size-dependence, $\varepsilon(d) \propto d^n, 2 \le \mathrm{n} \le 3$,[42] and in our case, $n = 2.5$ based on previous measurements.[20] The contribution to the PL made by Si nanocrystals of diameter *d*, depends on the relative optical absorption and the PL QY of the nanocrystals:

$$\mathrm{I(d)} = I_0(1 - 10^{-\varepsilon(d)N(d)CL})\mathrm{QY(d)} \quad (6)$$

$I_0$is the intensity of incident light at the excitation wavelength, *C* is the number concentration of Si nanocrystals, *L* is the light path length, $N(d)$, $\varepsilon(d)$ and QY(d) are size distribution, absorption cross section at the excitation wavelength and PL quantum yield of the Si nanocrystal with a diameter of d, respectively. Using a Taylor expansion of Eqn. 6,

$$\mathrm{I(d)} = \ln 10\, I_0 QY(d)[0 + \varepsilon(d)N(d)CL + {}^1\!/_2\,(\varepsilon(d)N(d)CL)^2 + \cdots] \quad (7)$$

and considering dispersions with low concentration ($\mathrm{C} \to 0$):

$$\mathrm{I(d)} = \ln 10\, I_0 QY(d)\varepsilon(d)N(d)CL \quad (8)$$

The observed average emission energy $\bar{E}(d)$ is

$$\bar{E}(d) = \frac{\sum_0^\infty I(d)E(d)}{\sum_0^\infty I(d)} = \frac{\sum_0^\infty I_0 QY(d)\varepsilon(d)N(d)CLE(d)}{\sum_0^\infty I_0 QY(d)\varepsilon(d)N(d)CL} = \frac{\sum_0^\infty QY(d)\varepsilon(d)N(d)E(d)}{\sum_0^\infty QY(d)\varepsilon(d)N(d)} \quad (9)$$

The number-average diameter is

$$\bar{d} = \frac{\sum_0^\infty N(d)d}{\sum_0^\infty \mathrm{N(d)}} = \sum_0^\infty N(d)d \Big/ N_{total} \quad (10)$$

Therefore, $E(\bar{d}) \neq \bar{E}(d)$ when the PL quantum yield and absorption cross section both depend on size. Figure 5 shows a comparison of calculated and experimentally measured PL energies. The data agree with the predicted values for the extended size range of average diameters from 1.8 nm and 9.1 nm. The PL of the Si nanocrystals can be predicted quite well using the EMA, even for nanocrystals smaller than 3 nm. One thing to note however is that the best EMA fitting corresponds to a 1.0 nm standard deviation, which is slightly larger than the actual standard deviation of the sample measured by SAXS, which is around 0.4~0.7 nm. The EMA model is slightly overestimating the optical gap in this size range.

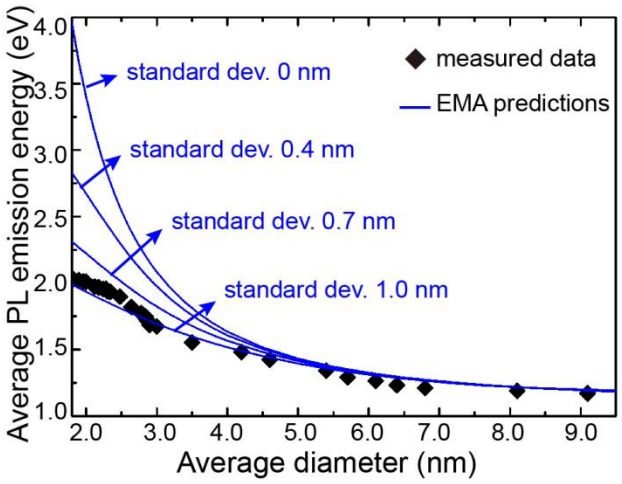

Figure 5. Average PL emission energy of Si nanocrystals predicted with the EMA by assuming a constant standard deviation for size distribution (blue curves) and the comparison with measured PL emission energy (black diamonds, same data shown in Figure 4b).

The time-resolved PL exhibits a bi-exponential decay (Figure 6a):[43]

$$\mathrm{I} = A_{fast}e^{-t/\tau_{fast}} + A_{slow}e^{-t/\tau_{slow}} \quad (11)$$

A_{fast} and A_{slow} are the relative numbers of excitons that decay through fast and slow channels, satisfying $A_{fast} + A_{slow} = 1$, τ_{fast} and τ_{slow} are the lifetimes of the fast and slow decays, respectively. The average PL lifetime, $\tau = A_{fast}\tau_{fast} + A_{slow}\tau_{slow}$, and radiative lifetime, $\tau_{Rad} = \tau/QY$, are in the range of tens to hundreds of microseconds, consistent with the indirect band gap of Si.[44,45] Figure 6b shows a plot of the PL lifetimes for nanocrystals of different size. The bi-exponential decay indicates that a significant number of fast nonradiative channels exist in the sample. As shown in Figure 6c, the relative fraction of fast nonradiative decay channels relative to the slower radiative decay pathways increase significantly as the nanocrystal size shrinks.

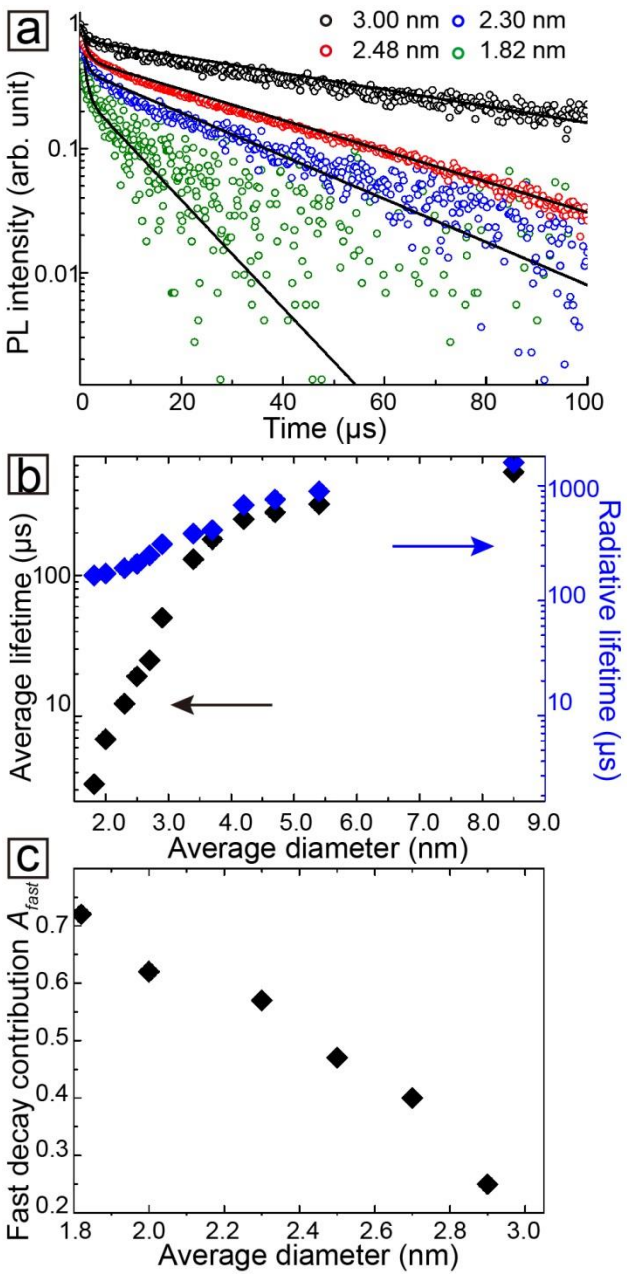

Figure 6. (a) PL decay data of Si nanocrystal population with various average diameters, which could be fitted by bi-exponential decay functions (black curves). The excitation wavelength is 371 nm and detection wavelength is 650 nm. (b) Plot of average PL lifetime and radiative lifetime for Si nanocrystals against average diameters. (c) Plot of fast decay contribution (A_{fast}) against average diameter, showing that there more excitons in smaller nanocrystals recombine through fast nonradiative channel, leading to the lower quantum yield.

Table 1. Summary of PL lifetime measurements and the parameters determined by fitting Eqn (11) to the data in Figure 6a for dodecene-capped Si nanocrystals in the small size range (< 3 nm).

Average diameter (nm)	Fast decay lifetime (μs)	Fast decay weight	Slow decay lifetime (μs)	Slow decay weight	Average lifetime (μs)
1.8	0.7	0.72	10	0.28	3.3
2.0	0.7	0.62	17	0.38	6.9
2.3	0.7	0.57	25	0.43	11.1
2.5	1.0	0.47	35	0.53	19.2
2.7	1.0	0.40	41	0.60	25.6
2.9	1.0	0.25	65	0.75	49.0

A decreased QY with decreasing diameter in the small size range has been observed for CdSe nanocrystals[45] and in other work for Si nanocrystals.[11] The loss in PL efficiency with decreased size has often been attributed to high surface defect densities. We checked for surface oxidation of the Si nanocrystals by XPS. As shown in Figure 7, XPS does show more pronounced oxidation of the smaller Si nanocrystals. Surface oxidation can reduce the QY, but oxidation does not necessarily lead to low PL efficiency. For example, Si nanocrystals embedded in SiO_2 substrates made by ion-implantation followed with thermal annealing have exhibited bright PL,[46,47] and nanocrystals linked to capping ligands by Si-O and Si-S bonds have also exhibited bright PL with similar quantum yield as alkyl passivated (Si-C) nanocrystals.[9,43,48]

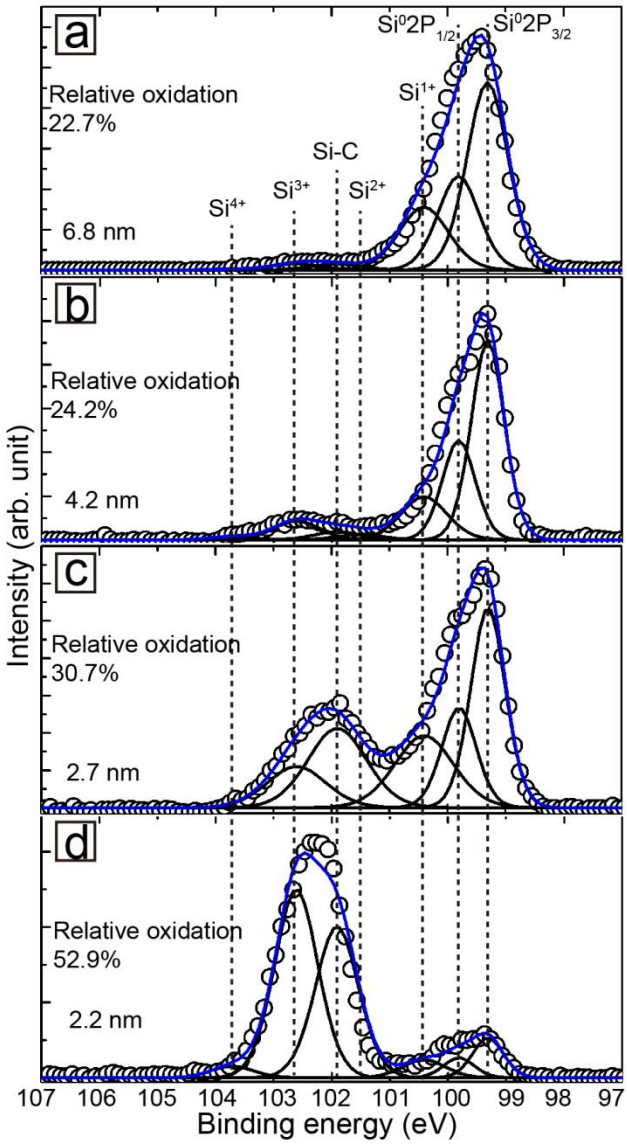

Figure 7. XPS Si 2p spectra of Si nanocrystal with average diameters of (a) 6.8 nm, (b) 4.2 nm, (c) 2.7 nm, and (d) 2.2 nm. The peak deconvolution shows relative contributions from zero valance Si ($Si^0 2P_{3/2}$ and $Si^0 2P_{1/2}$), Si-C bonding (Si-C), and various oxidation states (Si^{1+}, Si^{2+}, Si^{3+}, and Si^{4+}).

For the very small nanocrystals, there is an increasing probability that the exciton will interact with the nanocrystal surface and nonradiative channels such as defects on the surface or

vibrational modes of the capping ligands.[49] The probability of finding an exciton outside the nanocrystal depends on its wave function Ψ, which is obtained by solving the time independent Schrödinger equation:

$$\mathrm{H}\Psi = \mathrm{E}\Psi \tag{12}$$

We adopt the method developed by Kayanuma and Momiji.[50] and write the Hamilton as:

$$\mathrm{H} = E_g - \frac{\hbar^2}{2m_e}\left(\frac{\partial^2}{\partial r_e^2} + \frac{2}{r_e}\frac{\partial}{\partial r_e} + \frac{r_e^2 - r_h^2 + r_{e-h}^2}{r_e r_{e-h}}\frac{\partial^2}{\partial r_e \partial r_{e-h}}\right) - \frac{\hbar^2}{2m_h}\left(\frac{\partial^2}{\partial r_e^2} + \frac{2}{r_e}\frac{\partial}{\partial r_e} + \frac{r_e^2 - r_h^2 + r_{e-h}^2}{r_e r_{e-h}}\frac{\partial^2}{\partial r_e \partial r_{e-h}}\right) -$$

$$\frac{\hbar^2}{2\mu}\left(\frac{\partial^2}{\partial r_{e-h}^2} + \frac{2}{r_{e-h}}\frac{\partial}{\partial r_{e-h}}\right) - \frac{e^2}{\varepsilon r_{e-h}} + V_e(r_e) + V_h(r_h) \tag{13}$$

By using the Hylleraas coordinate system: $r_e \equiv |\overrightarrow{r_e}|, r_h \equiv |\overrightarrow{r_h}|, r_{e-h} \equiv |\overrightarrow{r_e} - \overrightarrow{r_h}|$. $\overrightarrow{r_e}$ and $\overrightarrow{r_h}$ are the positions of electron and hole, $E_g = 1.12\ eV$ is the band gap of bulk Si, m_e, m_e and μ are the effective mass of electron, hole, and the reduced effective mass of exciton, respectively. The potential function is described by

$$V_i(r_i) = \begin{cases} 0, r_i \le R \\ \overline{V_i}, r_i > R \end{cases}, i = e, h \tag{14}$$

$\overline{V_e}$ and $\overline{V_h}$ are the confining potentials for an electron and hole, satisfying $E_g + \overline{V_e} + \overline{V_h} = E_{environment}$, in which $E_{environment}$ is the energy difference between lowest unoccupied molecular orbital (LUMO) and highest occupied molecular orbital (HOMO) of 1-dodecene attached to Si nanocrystals. To approximate the energy levels associated with the alkyl chain on the Si surface, the HOMO-LUMO gap of alkyl thiols on a gold surface, [51,52] 4.5 eV, is used. For Si nanocrystals in the strong confinement regime, the electron and hole can be approximated as two non-interacting particles and the confining potentials for the electron and hole are assumed to be equal: $\overline{V_e} = \overline{V_h} = 0.5\left(E_{environment} - E_g\right) = 1.7eV$. The effective masses of the

electron and hole outside the nanocrystal is also taken to equal the value inside the nanocrystal. The trial wave function is:

$$\Psi(r_e, r_h, r_{e-h}) = A\phi_e(r_e)\phi_e(r_e)\, e^{(-r_{e-h}/\alpha)} \tag{15}$$

where $\phi_i(r_i) = \begin{cases} \sin(\beta_i r_i)/r_i, r_i \le R \\ B_i\, e^{(-\xi_i r_i)}/r_i, r_i > R \end{cases}, i = e, h$ (16)

A is the normalization constant, B_i and ξ_i could be expressed as a function of β_i and R based on the wave function smoothness at the nanocrystal boundary ($r_i = R$), β_e and β_h are variational parameters that are adjusted to minimize the expectation value of energy. The probability of finding an exciton outside the nanocrystal is

$$\rho_{outside\ nanocrystal} = 1 - \frac{\int_0^R dr_e \int_0^R dr_h \int_{|r_e - r_h|}^{|r_e + r_h|} dr_{e-h} \Psi\Psi^* r_e r_h r_{e-h}}{\int_0^\infty dr_e \int_0^\infty dr_h \int_{|r_e - r_h|}^{|r_e + r_h|} dr_{e-h} \Psi\Psi^* r_e r_h r_{e-h}} \tag{17}$$

Figure 8a shows the predictions made by this finite confinement model, which agree well with the data. Figure 8b shows the plot of the probability of finding an exciton outside the nanocrystal against the nanocrystal diameter for Si nanocrystals in the strong confinement regime. The probability of locating an exciton outside the nanocrystal increases as the nanocrystal becomes smaller. When an electron or hole is located outside the nanocrystal, it has a high likelihood of nonradiative recombination, leading to decreased QY. Figure 8c shows the probability an electron or hole will be located outside the nanocrystal and the corresponding (relative) QY.

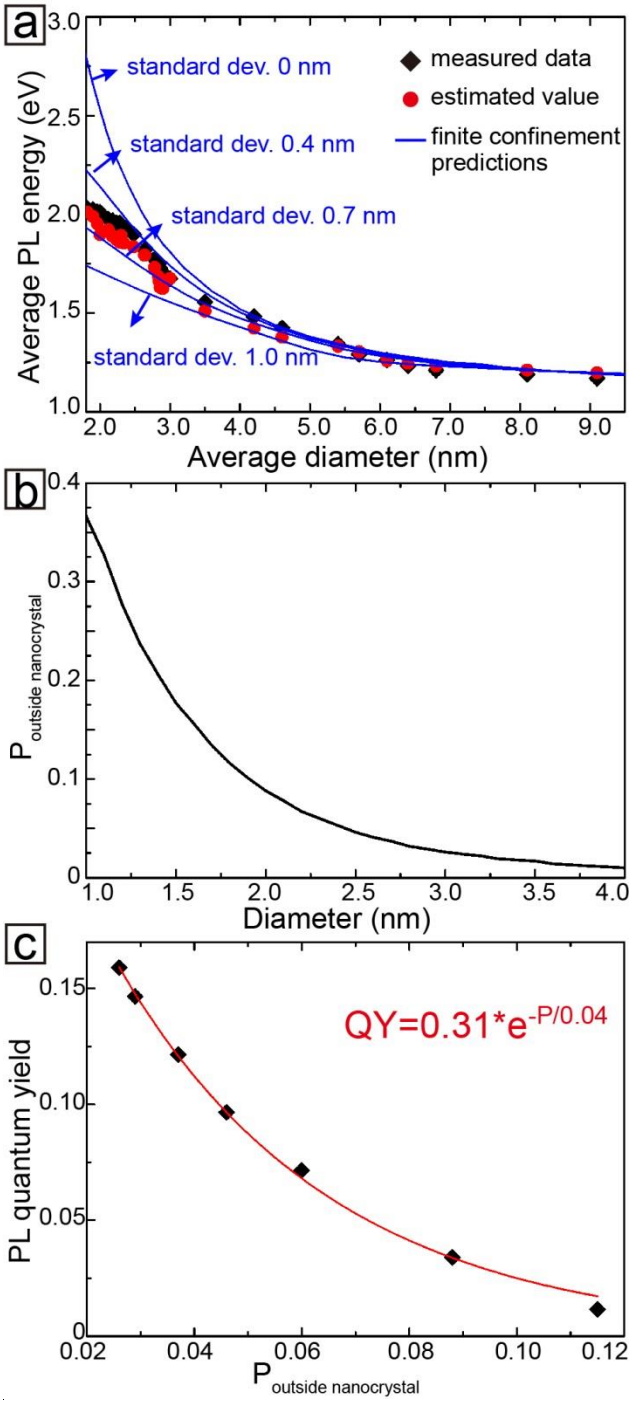

Figure 8. (a) PL emission energy (black diamonds) compared to predictions made by finite potential particle-in-box model with constant size standard deviations (blue curves), and red filled circles are estimated values of PL emission energy based on finite confinement energy and size distribution for each sample determined by solution SAXS (≤6.1 nm) or TEM (>6.1 nm). (b)

Plot of probability of finding electron or hole outside nanocrystal against nanocrystal size. (c) Correlation between probability of finding electron or hole outside nanocrystal and PL quantum yield, empirically fit to an exponential function.

CONCLUSIONS

In conclusion, the PL emission spectra and quantum yields, along with the average diameter and size distribution, were measured for a wide range of sizes of dodecene-capped Si nanocrystals. The size was determined using both TEM and SAXS to obtain the most accurate measurement possible. We show that with a proper accounting of the size-dependence of the PL QY and the optical absorption and the polydispersity of the nanocrystals that the EMA provides a reasonably accurate correlation between size and optical gap. A finite confinement model for the exciton provides an explanation for the observed drop in PL QY and increased nonradiative recombination with decreased size when the nanocrystals are smaller than about 3 nm in diameter. It should be possible to significantly increase the PL QY of the smaller Si nanocrystals by developing an effective inorganic shell passivation strategy, similar to what has been done for CdSe.[53, 54]

Supporting Information

Histograms of nanocrystal diameter obtained from TEM images; SAXS data used to determine the Si nanocrystal size; FTIR, PL excitation, and PL decay data for Si nanocrystals; derivation of the finite confinement model. This material is available free of charge via the internet at http://pubs.acs.org.

Acknowledgements

Financial support of this work was provided by the Robert A. Welch Foundation (Grant no. F-1464), the National Science Foundation (Grant no. CHE-1308813), and European Commission ERC Starting Grant (PhotoSi, 278912). The Cornell High Energy Synchrotron Source (CHESS) is a national user facility supported by the National Science Foundation under award DMR-1332208.

References

(1) Miller, J. B.; Van Sickle, A. R.; Anthony, R. J.; Kroll, D. M.; Kortshagen, U. R.; Hobbie, E. K. Ensemble Brightening and Enhanced Quantum Yield in Size-Purified Silicon Nanocrystal. *ACS Nano* **2012**, *6*, 7389-7396.

(2) Hessel, C. M.; Rasch, M. R.; Hueso, J. L.; Goodfellow, B. W.; Akhavan, V. A.; Puvanakrishnan, P.; Tunnel, J. W.; Korgel, B. A. Alkyl Passivation and Amphiphilic Polymer Coating of Silicon Nanocrystals for Diagnostic Imaging. *Small* **2010**, *6*, 2026-2034.

(3) Sugimoto, H.; Hori, Y.; Imura, Y.; Fujii, M. Charge-Transfer-Induced Photoluminescence Enhancement in Colloidal Silicon Quantum Dots. *J. Phys. Chem. C* **2017**, *121*, 11962-11967.

(4) Greben, M.; Khoroshyy, P.; Liu, X.; Pi, X.; Valenta, J. Fully Radiative Relaxation of Silicon Nanocrystals in Colloidal Ensemble Revealed by Advanced Treatment of Decay Kinetics. *J. Appl. Phys.* **2017**, *122*, 034304.

(5) Lee, B. G.; Luo, J.-W.; Neale, N. R.; Beard, M. C.; Hiller, D.; Zacharias, M.; Stradins, P.; Zunger, A. Quasi-Direct Optical Transitions in Silicon Nanocrystals with Intensity Exceeding the Bulk. *Nano Lett.* **2016**, *16*, 1583-1589.

(6) Brown, S. L.; Vogel, D. J.; Miller, J. B.; Inerbaev, T. M.; Anthony, R. J.; Kortshagen, U. R.; Kilin, D. S.; Hobbie, E. K. Enhancing Silicon Nanocrystal Photoluminescence through Temperature and Microstructure. *J. Phys. Chem. C* **2016**, *120*, 18909-18916.

(7) Clark, R. J.; Aghajamali, M.; Gonzalez, C. M.; Hadidi, L.; Islam, M. A.; Javadi, M.; Hosnay Mobarak, M.; Purkait, T. K.; Robidillo, C. J. T.; Sinelnikov, R.; Thiessen, A. N.; Washington, J.; Yu, H.; Veinot, J. G. C. From Hydrogen Silsesquioxane to Functionalized Silicon Nanocrystals. *Chem. Mater.* **2017**, *29*, 80-89.

(8) Stolle, C. J.; Lu, X.; Yu, Y.; Schaller, R. D.; Korgel, B. A. Efficient Carrier Multiplication in Colloidal Silicon Nanorods. *Nano Lett.* **2017**, ASAP Contents.

(9) Sinelnikov, R.; Dasog, M.; Beamish, J.; Meldrum, A.; Veinot, J. G. C. Revisiting an Ongoing Debate: What Role Do Surface Groups Play in Silicon Nanocrystal Photoluminescence? *ACS Photonics* **2017**, ASAP Contents.

(10) Locritani, M.; Yu, Y.; Bergamini, G.; Baroncini, M.; Molloy, J. K.; Korgel, B. A.; Ceroni, P. Silicon Nanocrystals Functionalized with Pyrene Units: Efficient Light-Harvesting Antennae with Bright Near-Infrared Emission. *J. Phys. Chem. Lett.* **2014**, *5*, 3325-3329.

(11) Mastronardi, M. L.; Maier-Flaig, F.; Faulkner, D.; Henderson, E. J.; Kübel, C.; Lemmer, U.; Ozin, G. A. Size-Dependent Absolute Quantum Yields for Size-Separated Colloidally-Stable Silicon Nanocrystals. *Nano Lett.* **2012**, *12*, 337-342.

(12) Moskalenko, A. S.; Berakdar, J.; Prokofiev, A. A.; Yassievich, I. N.; Single-Particle States in Spherical Si/SiO_2 Quantum Dots. *Phys. Rev. B* **2007**, *76*, 085427.

(13) Sychugov, I, Juhasz, R.; Valenta, J.; Linnros, J. Narrow Luminescence Linewidth of a Silicon Quantum Dot. *Phys. Rev. Lett.* **2005**, *94*, 087405.

(14) Mangolini, L.; Jurbergs, D.; Rogojina, E.; Kortshagen, U. Plasma Synthesis and Liquid Surface Passivation of Brightly Luminescent Si Nanocrystals. *J. Lumin.* **2006**, *121*, 327-334.

(15) Yu, Y.; Lu, X.; Guillaussier, A.; Reddy Voggu, R.; Pineros, W.; de la Mata, M.; Arbiol, J.; Smilgies, D.-M.; Truskett, T. M.; Korgel, B. A. Orientationally Ordered Silicon Nanocrystal Cuboctahedra in Superlattices. *Nano Lett.* **2016**, *16*, 7814-7821.

(16) Yu, Y.; Bosoy, C. A.; Hessel, C. M.; Smilgies, D.-M.; Korgel, B. A. Silicon Nanocrystal Superlattices. *ChemPhysChem* **2013**, *14*, 84-87.

(17) Yu, Y.; Bosoy, C. A.; Smilgies, D.-M.; Korgel, B. A. Self-Assembly and Thermal Stability of Binary Superlattices of Gold and Silicon Nanocrystals. *J. Phys. Chem. Lett.* **2013**, *4*, 3677-3682.

(18) Jurbergs, D.; Rogojina, E.; Mangolini, L.; Kortshagen, U. Silicon Nanocrystals with Ensemble Quantum Yields Exceeding 60%. *Appl. Phys. Lett.* **2006**, *88*, 233116.

(19) Dasog, M.; Yang, Z.; Regli, S.; Atkins, T. M.; Faramus, A.; Singh, M. P.; Muthuswamy, E.; Kauzlarich, S. M.; Tilley, R. D.; Veinot, J. G. C. Chemical Insight into the Origin of Red and Blue Photoluminescence Arising from Freestanding Silicon Nanocrystals. *ACS Nano* **2013**, *7*, 2676-2685.

(20) Hessel, C. M.; Reid, D.; Panthani M. G.; Rasch, M. R.; Goodfellow, B. W.; Wei, J.; Fujii, H.; Akhavan, V.; Korgel, B. A. Synthesis of Ligand-Stabilized Silicon Nanocrystals with Size-Dependent Photoluminescence Spanning Visible to Near-Infrared Wavelengths. *Chem. Mater.* **2012**, *24*, 393-401.

(21) Dasog, M.; De, I. R.; Titova, L. V.; Hegmann, F. A.; Veinot, J. G. C. Size vs Surface: Tuning the Photoluminescence of Freestanding Silicon Nanocrystals Across the Visible Spectrum via Surface Groups. *ACS Nano* **2014**, *8*, 9636-9648.

(22) Gu, L.; Hall, D. J.; Qin, Z.; Anglin, E.; Joo, J.; Mooney, D. J.; Howell, S. B.; Sailor, M. J. *In vivo* Time-Gated Fluorescence Imaging with Biodegradable Luminescent Porous Silicon Nanoparticles. *Nat. Commun.* **2012**, *4*, 2326.

(23) Erogbogbo, R.; Yong, K.-T.; Roy, I.; Xu, G.; Prasad, P. N.; Swihart, M. T. Biocompatible Luminescent Silicon Quantum Dots for Imaging of Cancer Cells. *ACS Nano* **2008**, *2*, 873-878.

(24) Puzzo, D. P.; Henderson, E. J.; Helander, M. G.; Wang, Z.; Ozin, G. A.; Lu, Z. Visible Colloidal Nanocrystal Silicon Light-Emitting Diode. *Nano Lett.* **2011**, *11*, 1585-1590.

(25) Cheng, K.-Y.; Anthony, R.; Kortshagen, U. R.; Holmes, R. J. High-Efficiency Silicon Nanocrystal Light-Emitting Devices. *Nano Lett.* **2011**, *11*, 1952-1956.

(26) Gu, W.; Liu, X.; Pi, X.; Dai, X.; Zhao, S.; Yao, L.; Li, D.; Jin, Y.; Xu, M.; Yang, D.; Qin, G. Silicon-Quantum-Dot Light-Emitting Diodes With Interlayer-Enhanced Hole Transport. *IEEE Photonics J.* **2017**, *9*, 4500610.

(27) Meinardi, F.; Ehrenberg, S.; Dhamo, L.; Carulli, F.; Mauri, M.; Bruni, F.; Simonutti, R.; Korthagen, U.; Brovelli, S. "Highly Efficient Luminescent Solar Concentrators Based on Earth-Abundant Indirect-Bandgap Silicon Quantum Dots," *Nature Photonics* **2017**, *11*, 177-186.

(28) Liu, X.; Zhang, Y.; Yu, T.; Qiao, X.; Gresback, R.; Pi, X.; Yang, D. Optimum Quantum Yield of the Light Emission from 2 to 10 nm Hydrosilylated Silicon Quantum Dots, *Part. Part. Syst. Charact.* **2016**, *33*, 44-52.

(29) Wen, X.; Zhang, P.; Smith, T. A.; Anthony, R. J.; Kortshagen, U. R.; Yu, P.; Feng, Y.; Shrestha, S.; Coniber, G.; Huang, S. Tunability Limit of Photoluminescence in Colloidal Silicon Nanocrystals. *Sci. Rep.* **2015**, *5*, 12469.

(30) Kayanuma, Y. Wannier Exciton in Microcrystals. *Solid State Commun.* **1986**, *59*, 405-408.

(31) Bawendi, M. G.; Steigerwald, M. L.; Brus, L. E. The Quantum Mechanics of Larger Semiconductor Clusters ("Quantum Dots") *Annu. Rev. Phys. Chem.* **1990**, *41*, 477-496.

(32) Schuppler, S.; Friedman, S. L.; Marcus, M. A.; Alder, D. L.; Xie, Y.-H.; Ross, F. M.; Harris, T. D.; Brown, W. L.; Chabal, Y. J.; Brus, L. E.; Citrin, P. H. Dimensions of Luminescent Oxidized and Porous Silicon Structures. *Phys. Rev. Lett.* **1994**, *72*, 2648-2651.

(33) von Behren, J.; van Buuren, T.; Zacharias, M.; Chimowitz, E. H.; Fauchet, P. M. Quantum Confinement in Nanoscale Silicon: The Correlation of Size with Bandgap and Luminescence. *Solid State Commun.* **1998**, *105*, 317-322.

(34) Hill, N. A.; Whaley, K. B. Size Dependence of Excitons in Silicon Nanocrystals. *Phys. Rev. Lett.* **1995**, *75*, 1130-1133.

(35) Sée, J.; Dollfus, P.; Galdin, S. Comparison between a sp^3d^5 Tight-Binding and an Effective Mass Description of Silicon Quantum Dots. *Phys. Rev. B* **2002**, *66*, 193307.

(36) Wolkin, M. V.; Jorne, J.; Fauchet, P. M.; Allan, G.; Delerue, C. Electronic States and Luminescence in Porous Silicon Quantum Dots: The Role of Oxygen. *Phys. Rev. Lett.* **1999**, *82*, 197-200.

(37) Panthani, M. G.; Hessel, C. M.; Reid, D.; Casillas, G.; José-Yacamán, M.; Korgel, B. A. Graphene-Supported High Resolution TEM and STEM Imaging of Silicon Nanocrystals and their Capping Ligands. *J. Phys. Chem. C* **2012**, *116*, 22463-22468.

(38) Saunders, A. E.; Sigman, M. B.; Korgel, B. A. Growth Kinetics and Metastability of Mondisperse Tetraoctylammonium Bromide Capped Gold Nanocrystals. *J. Phys. Chem. B* **2004**, *108*, 193-199.

(39) de Mello, J. C.; Wittmann, H. F.; Friend R. H. An Improved Experimental Determination of External Photoluminescence Quantum Efficiency. *Adv. Mater.* **1997**, *9*, 230-232.

(40) Goodfellow, B. W.; Rasch, M. R.; Hessel, C. M.; Patel, R. N.; Smilgies, D.-M.; Korgel, B. A. Ordered Structure Rearrangements in Heated Gold Nanocrystal Superlattices. *Nano Lett.* **2013**, *13*, 5710-5714.

(41) Kovalev, D; Diener,J.; Heckler,H.; Polisski, G.; Künzner, N.; Koch, F. Optical Absorption Cross Sections of Silicon Nanocrystals *Phys. Rev. B* **2000**, *61*, 4485.

(42) Yu, W. W.; Qu, L.; Guo, W.; Peng, X. Experimental Determination of the Extinction Coefficient of CdTe, CdSe, and CdS Nanocrystals. *Chem. Mater.* **2003**, *15*, 2854-2860.

(43) Yu, Y.; Rowland, C. E.; Schaller, R. D.; Korgel, B. A. Synthesis and Ligand Exchange of Thiol-Capped Silicon Nanocrystals. *Langmuir* **2015**, *31*, 6886-6893.

(44) Schlangenotto, H.; Maeder, H.; Gerlach, W. Temperature Dependence of the Radiative Recombination Coefficient in Silicon. *Phys. Stat. Sol. (a)* **1974**, *21*,357-367.

(45) Qu, L.; Peng, X. Control of Photoluminescence Properties of CdSe Nanocrystals in Growth. *J. Am. Chem. Soc.* **2002**, *124*, 2049-2055

(46) Pavesi, L.; Dal Negro, L.; Mazzoleni, C.; Franzò, G.; Paiolo, F. Optical Gain in Silicon Nanocrystals *Nature* **2000**, *408*, 440-444.

(47) Brus, L. "Luminescence of Silicon Materials: Chains, Sheets, Nanocrystals, Nanowires, Microcrystals, and Porous Silicon," *J. Phys. Chem.* **1994**, *98*, 3575-3581.

(48) Anderson, R. T.; Zang, X.; Fernando, R.; Dzara, M. J.; Ngo, C.; Sharps, M.; Pinals, R.; Pylypenko, S.; Lusk, M. T.; Sellinger, A. Direct Conversion of Hydride- to Siloxane-Terminated Silicon Quantum Dots. *J. Phys. Chem. C* **2016**, *120*, 25822-25831.

(49) Lifshitz, E. Evidence in Support of Exciton to Ligand Vibrational Coupling in Colloidal Quantum dots. *J. Phys. Chem. Lett.* **2015**, *6*, 4336-4347.

(50) Kanyanuma, Y.; Momiji, H.; Incomplete Confinement of Electrons and Holes in Microcrystals. *Phys. Rev. B* **1990**, *41*, 10261-10263.(51) Xue, Y.; Datta, S.; Ratner, M. A. Charge Transfer and "Band Lineup" in Molecular Electronic Devices: A Chemical and Numerical Interpretation. *J. Chem. Phys.* **2001**, *115*, 4292-4299.

(52) Liu, Y.; Gibbs, M.; Puthussery, J.; Gaik, S.; Ihly, R.; Hillhouse, H. W.; Law, M. Dependence of Carrier Mobility on Nanocrystal Size and Ligand Length in PbSe Nanocrystal Solids. *Nano Lett.* **2010**, *10*, 1960-1969.

(53) Dabbousi, B. O.; Rodriguez-Viejo, J.; Mikulec, F. V.; Heine, J. R.; Mattoussi, H.; Ober, R.; Jensen, K. F.; Bawendi, M. G. (CdSe)ZnS Core-Shell Quantum Dots: Synthesis and Characterization of a Size Series of Highly Luminescent Nanocrystallites. *J. Phys. Chem. B* **1997**, *101*, 9463-9475.

(54) Hines, M. A.; Guyot-Sionnest, P. Synthesis and Characterization of Strongly Luminescing ZnS-Capped CdSe Nanocrystals. *J. Phys. Chem.* **1996**, *100*, 468-471.

TOC Figure:

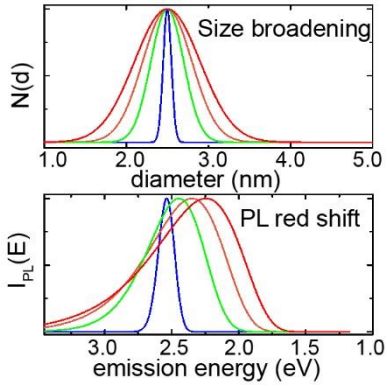
Size broadening
N(d)
1.0
2.0
3.0
4.0
5.0
diameter (nm)
PL red shift
$I_{PL}(E)$
3.0
2.5
2.0
1.5
1.0
emission energy (eV)